https://doi.org/10.5194/egusphere-2026-3672
Preprint. Discussion started: 22 July 2026


# Time averaging for tendency budget analysis

Christopher Bladwell[1,2,3], Ryan M. Holmes[1,3], Jan D. Zika[2,4], Stephen M. Griffies[5,6], and Andrew E. Kiss[7]

[1]Bureau of Meteorology, Melbourne, Victoria, Australia
[2]School of Mathematics and Statistics, University of New South Wales
[3]School of Geosciences, University of Sydney, Sydney, New South Wales, Australia
[4]ARC Australian Centre for Excellence in Antarctic Science (ACEAS), University of New South Wales, Sydney, New South Wales, Australia
[5]Sorbonne Université-CNRS-IRD-MNHN, LOCEAN Laboratory, Paris, France
[6]Princeton University Program in Atmospheric and Oceanic Sciences, Princeton, NJ, USA
[7]Research School of Earth Sciences, Australian National University, Canberra, ACT, Australia

**Correspondence:** Christopher Bladwell (christopher.bladwell@bom.gov.au)

**Abstract.** Climate models can be used to quantify the processes that contribute to a property's change through analysis of the tendency terms in the budget of the property. For example, a heat budget can be performed to understand the processes driving an increase in the ocean's heat content under climate change. However, conventional budget analyses in climate models are typically performed without proper consideration of their relationship to the property of interest. Specifically, most studies consider standard arithmetic time-averages of budget terms. For the tendency term, this average is related to the difference between two time instants (snapshots) of the property and thus is strongly impacted by rapid fluctuations, or "weather". Such an approach to budget analysis is thus less relevant to the "climate change" problem, that is, the difference between two long-term averages, or "epochs", of the property. Here we present a time-averaging method, referred to as the *hat average*, which exactly relates the processes contributing to a property's tendency budget to the epoch difference, or "climate change", of that property. We demonstrate the utility of this method by applying it to the horizontally integrated heat budget of a global ocean model. We find that the hat average removes high-frequency variability, typically associated with rapid and noisy advective processes, and so allows for a clear measure of how processes contribute to changes in climate.

## 1 Introduction

In many scientific disciplines it is common to perform tendency budget analyses within numerical models to measure how different physical processes contribute to the tendency (time derivative) of a property. These analyses are typically performed with model budget terms which are arithmetically averaged over a particular time period. However, a limitation of this method is that a standard, or *boxcar*, arithmetic time-average of the tendency term amounts to a difference between the *instantaneous* values of the property at the beginning and end of the time averaging period, rather than to a difference of time averages of the

https://doi.org/10.5194/egusphere-2026-3672
Preprint. Discussion started: 22 July 2026


property. The difference of instantaneous snapshots is strongly impacted by high-frequency variability, so that the balance of processes that drive changes in the snapshots may differ quantitatively and qualitatively from the processes that drive long-term trends.

Here we are concerned with the specific example of quantifying the processes that govern changes in the Earth's climate and weather. Climate, the long-term average state of weather, is distinct from weather, the high-frequency variability. A common approach to separate climate trends from weather is to take differences in the property of interest averaged over two epochs at the beginning and the ending of the period of interest, an "epoch difference" (Ding and Steig, 2013; Barnes and Barnes, 2015). Epoch differences have been shown to produce similar results to linear regressions in studies using observational data (Ding and Steig, 2013) and numerical climate simulations (Deser et al., 2012; Kravitz et al., 2017), given a suitable choice of epoch lengths. The use of averages in the epoch difference damps out the weather variability at shorter time-scales, isolating the climate trend.

Numerical climate models not only allow us to project future climate change, but also to understand the processes that drive those changes. Budget analyses, such as heat (enthalpy) and salt budgets for the ocean or heat and moisture budgets for the atmosphere, allow the change in heat, salt, and water content to be attributed to individual processes such as air-sea heat fluxes, advective transport, irreversible mixing, or localized sources. For example, ocean budget analyses have been used to understand how advection by mean flows, diffusion and eddy-transport move anomalous heat absorbed at the sea surface into the ocean interior (Gregory, 2000; Wolfe et al., 2008; Morrison et al., 2013; Palter et al., 2014; Griffies et al., 2015; Dias et al., 2020), or what processes are responsible for different aspects of sea level variability (Griffies and Greatbatch, 2012; Piecuch and Ponte, 2014).

Studies have shown that the balance of terms responsible for driving property change depends on the time-scale considered. For example, Holmes et al. (2022) found that high-frequency variability in horizontally-averaged ocean heat content in a free running climate model was dominated by advection, while mixing became far more important at decadal-centennial time scales. This time scale separation between fast (typically reversible) processes and slow (typically irreversible) processes is central to ocean climate dynamics, and so a method to isolate the budget contributions to changes on both slow and fast time-scales is needed.

Here we describe a time-averaging method, referred to as the *hat average*, that quantifies the contributions of budget processes to the epoch difference of a property. The hat average is based on an idea introduced by Oerder et al. (2016) who used a double time integral of the momentum budget to quantify processes that drive time-averaged wind speed anomalies in a regional atmosphere-ocean model. We here offer a detailed discussion of this method, and provide further context for its importance for addressing central questions of climate change, with an emphasis on the ocean.

We derive the hat average mathematically in Section 2, with the presentation emphasizing the difference between the hat average and the standard boxcar time average. We demonstrate the utility of the hat average by measuring how processes drive ocean heat content change in an ocean climate model (Sections 3 and 4). In Section 5 we discuss the strengths and weaknesses of the approach using a box model of the climate system as an example, and then we offer conclusions in Section 6. In Appendix

https://doi.org/10.5194/egusphere-2026-3672
Preprint. Discussion started: 22 July 2026


A we derive the double integral identity that is central to the hat average, with this identity originally due to Cauchy (1823). We provide additional information about the numerical implementation of the hat average in Appendix B.

## 2 Budget analysis and epoch differences

In this section we introduce the initial value problem for a general time dependent property $\xi = \xi(\mathbf{x}, t)$ and its epoch difference, which isolates the long-term trend in $\xi$ from high-frequency variability. We then present the hat-averaged budget which relates the epoch difference of $\xi$ to individual processes.

### 2.1 Budget of a variable and its epoch difference

Consider a generic budget equation for the time evolution of a property, $\xi = \xi(\mathbf{x}, t)$, given by

$$\frac{\partial \xi}{\partial t} = \sum_{i=1}^{n} f_i(\mathbf{x}, t), \tag{1}$$

where $\mathbf{x}$ is the spatial position, $t$ is time, and $f_i(\mathbf{x}, t)$, $i = 1, .., n$, denotes a suite of $n$ processes that contribute to the time tendency of $\xi$. For example, $\xi(\mathbf{x}, t)$ could represent the ocean's heat content, with $f_i$ representing contributions to its tendency from advection, diffusion, surface heat fluxes and other processes. Time integrating Eq. (1) over a time period $[t_a, t_b]$ relates the sum of the processes $f_i$ to the difference between the instantaneous value of $\xi$ at the final time, $t = t_b$, and the initial time, $t = t_a$,

$$\xi(\mathbf{x}, t_b) - \xi(\mathbf{x}, t_a) = \int_{t_a}^{t_b} \frac{\partial \xi}{\partial t} \, \mathrm{d}t = \int_{t_a}^{t_b} \sum_{i=1}^{n} f_i(\mathbf{x}, t) \, \mathrm{d}t. \tag{2}$$

The instantaneous snapshot difference of $\xi$ characterized by Eq. (2) is typically of less interest than the difference in time-average quantities, as quantified for example by the epoch difference between the time average of $\xi$ computed over a time epoch $[t_1, t_1 + \Delta t]$ and an earlier epoch $[t_0, t_0 + \Delta t]$,

$$\overline{\xi}_{t_1, t_1+\Delta t} - \overline{\xi}_{t_0, t_0+\Delta t} = \frac{1}{\Delta t} \int_{t_1}^{t_1+\Delta t} \xi(\mathbf{x}, t) \, \mathrm{d}t - \frac{1}{\Delta t} \int_{t_0}^{t_0+\Delta t} \xi(\mathbf{x}, t) \, \mathrm{d}t, \tag{3}$$

where the overline denotes the unweighted time average between the two times given as subscripts. This epoch difference is illustrated for an example quantity $\xi$ in Fig. 1a by the difference in average of $\xi$ over the periods shown in green (connected by the green dashed curve). This epoch difference is more representative of the change in climate between the two periods than the snapshot difference taken at the midpoint of each of the epochs (the red dotted line in Fig. 1a), captured by Eq. (2) with $t_b = t_1 + \Delta t/2$ and $t_a = t_0 + \Delta t/2$. Note that the rate of change of $\xi$ with time corresponding to either the epoch difference or snapshot difference can be obtained by dividing the difference by the elapsed time, $t_b - t_a$.

While the epoch difference is more representative of the change in climate than a snapshot difference, how the various processes, $f_i$, contribute to this epoch difference is less obvious. Here we use a method presented in Oerder et al. (2016) to relate the processes driving the time tendency of a general property to its epoch difference.

https://doi.org/10.5194/egusphere-2026-3672
Preprint. Discussion started: 22 July 2026


We begin by first considering a single epoch $[t_1, t_1 + \Delta t]$. Integrating Eq. (1) to some $t \in [t_1, t_1 + \Delta t]$, we obtain

$$\xi(\mathbf{x},t) - \xi(\mathbf{x},t_1) = \int_{t_1}^{t} \frac{\partial \xi}{\partial t'}\,\mathrm{d}t' = \int_{t_1}^{t} \sum_i f_i(\mathbf{x},t')\,\mathrm{d}t'. \tag{4}$$

Using Eq. (4) we can rewrite the epoch average of $\xi$ as

$$\overline{\xi}_{t_1,t_1+\Delta t} = \frac{1}{\Delta t}\int_{t_1}^{t_1+\Delta t} \xi(\mathbf{x},t)\,\mathrm{d}t = \xi(\mathbf{x},t_1) + \frac{1}{\Delta t}\int_{t_1}^{t_1+\Delta t}\int_{t_1}^{t} \frac{\partial \xi}{\partial t'}\,\mathrm{d}t'\,\mathrm{d}t. \tag{5}$$

Substituting Eq. (5) (applied over both the initial and final epochs) into Eq. (3) yields

$$\begin{aligned}\overline{\xi}_{t_1,t_1+\Delta t} - \overline{\xi}_{t_0,t_0+\Delta t} &= \frac{1}{\Delta t}\int_{t_1}^{t_1+\Delta t}\int_{t_1}^{t} \frac{\partial \xi}{\partial t'}\,\mathrm{d}t'\,\mathrm{d}t + \xi(\mathbf{x},t_1) - \xi(\mathbf{x},t_0) - \frac{1}{\Delta t}\int_{t_0}^{t_0+\Delta t}\int_{t_0}^{t} \frac{\partial \xi}{\partial t'}\,\mathrm{d}t'\,\mathrm{d}t \\ &= \frac{1}{\Delta t}\int_{t_1}^{t_1+\Delta t}\int_{t_1}^{t} \frac{\partial \xi}{\partial t'}\,\mathrm{d}t'\,\mathrm{d}t + \int_{t_0}^{t_1} \frac{\partial \xi}{\partial t}\,\mathrm{d}t - \frac{1}{\Delta t}\int_{t_0}^{t_0+\Delta t}\int_{t_0}^{t} \frac{\partial \xi}{\partial t'}\,\mathrm{d}t'\,\mathrm{d}t,\end{aligned} \tag{6}$$

which defines a relationship between the epoch difference of the variable $\xi$ and its time tendency [or the sum of budget processes $f_i$, via Eq. (1)].

### 2.2 Simplification of the double integrals

We can simplify the double integrals in Eq. (6) by making use of the following identity, which is a particular case of the Cauchy (1823) repeated integral formula (see Appendix A for a derivation)

$$\int_{a}^{x}\int_{a}^{t} g(t')\,\mathrm{d}t'\,\mathrm{d}t = \int_{a}^{x} (x-t)\,g(t)\,\mathrm{d}t. \tag{7}$$

Applying Cauchy's formula (7) to the double integrals in Eq. (6) yields

$$\begin{aligned}\overline{\xi}_{t_1,t_1+\Delta t} - \overline{\xi}_{t_0,t_0+\Delta t} = &\int_{t_1}^{t_1+\Delta t} \left(\frac{t_1+\Delta t - t}{\Delta t}\right)\frac{\partial \xi}{\partial t}\,\mathrm{d}t + \int_{t_0}^{t_1} \frac{\partial \xi}{\partial t}\,\mathrm{d}t \\ &- \int_{t_0}^{t_0+\Delta t} \left(\frac{t_0+\Delta t - t}{\Delta t}\right)\frac{\partial \xi}{\partial t}\,\mathrm{d}t.\end{aligned} \tag{8}$$

https://doi.org/10.5194/egusphere-2026-3672
Preprint. Discussion started: 22 July 2026


This equation can be written in another form,

$$\begin{aligned}
\overline{\xi}_{t_1,t_1+\Delta t} - \overline{\xi}_{t_0,t_0+\Delta t} &= \int\limits_{t_1}^{t_1+\Delta t} \left(\frac{t_1+\Delta t - t}{\Delta t}\right)\frac{\partial \xi}{\partial t}\,\mathrm{d}t + \int\limits_{t_0+\Delta t}^{t_1} \frac{\partial \xi}{\partial t}\,\mathrm{d}t \\
&\quad + \int\limits_{t_0}^{t_0+\Delta t} \left[\frac{\partial \xi}{\partial t} - \left(\frac{t_0+\Delta t - t}{\Delta t}\right)\frac{\partial \xi}{\partial t}\right]\mathrm{d}t \\
&= \int\limits_{t_0}^{t_0+\Delta t} \left(\frac{t-t_0}{\Delta t}\right)\frac{\partial \xi}{\partial t}\,\mathrm{d}t + \int\limits_{t_0+\Delta t}^{t_1} \frac{\partial \xi}{\partial t}\,\mathrm{d}t \\
&\quad + \int\limits_{t_1}^{t_1+\Delta t} \left(\frac{t_1+\Delta t - t}{\Delta t}\right)\frac{\partial \xi}{\partial t}\,\mathrm{d}t.
\end{aligned} \tag{9}$$

In this form the epoch difference of $\xi$ is equal to a "rising" linear weighted integral over the initial epoch (with a weighting $(t-t_0)/\Delta t$) and a "falling" linear weighted integral over the final epoch (with a weighting $(t_1+\Delta t-t)/\Delta t$), plus the unweighted integral of the tendency over the period between the epochs. Due to the rising value of the weighting function over the initial epoch and the falling value of the weighting over the final epoch, we refer to this equation as the *hat* weighted integral of the tendency of $\xi$. The unit weighting of the boxcar average is shown by the shaded area in Figure 1b, while the hat weighting is shown by the shaded area in Figure 1c.

The above discussion shows that to precisely relate the epoch difference of a property to its process based tendencies, hat averaging must be used. Taking the hat average of tendencies in a numerical model is not substantially more involved than taking a boxcar average, but does require saving additional diagnostics – namely the rising-weighted average of each tendency in addition to the standard boxcar average (note that the falling average can be obtained by subtracting the rising average from the standard average). From these saved boxcar and rising averages, the hat average for all relevant epoch differences can be computed as a post-processing step (as long as the epoch difference length can be formed as a simple combination of the time-averaging periods of the diagnostics). The specific epoch periods of interest do not have to be specified $a\ priori$, nor are model snapshots or restarts required. The specific details of this procedure are discussed in Appendix B.

### 2.3 Interpretation in the frequency domain

Further insight into the hat-average is gained by examining the effect of both averaging methods in the frequency domain. We discuss this interpretation in this section.

The accumulation of budget diagnostics by time-averaging over some finite time period (say, a month for definiteness) is equivalent to a monthly sampling of the convolution of a window function and the tendency budget diagnostic $f$, given by

$$w(t) * f(t) = \int\limits_{-\infty}^{\infty} w(t-t')f(t')\mathrm{d}t', \tag{10}$$

https://doi.org/10.5194/egusphere-2026-3672
Preprint. Discussion started: 22 July 2026


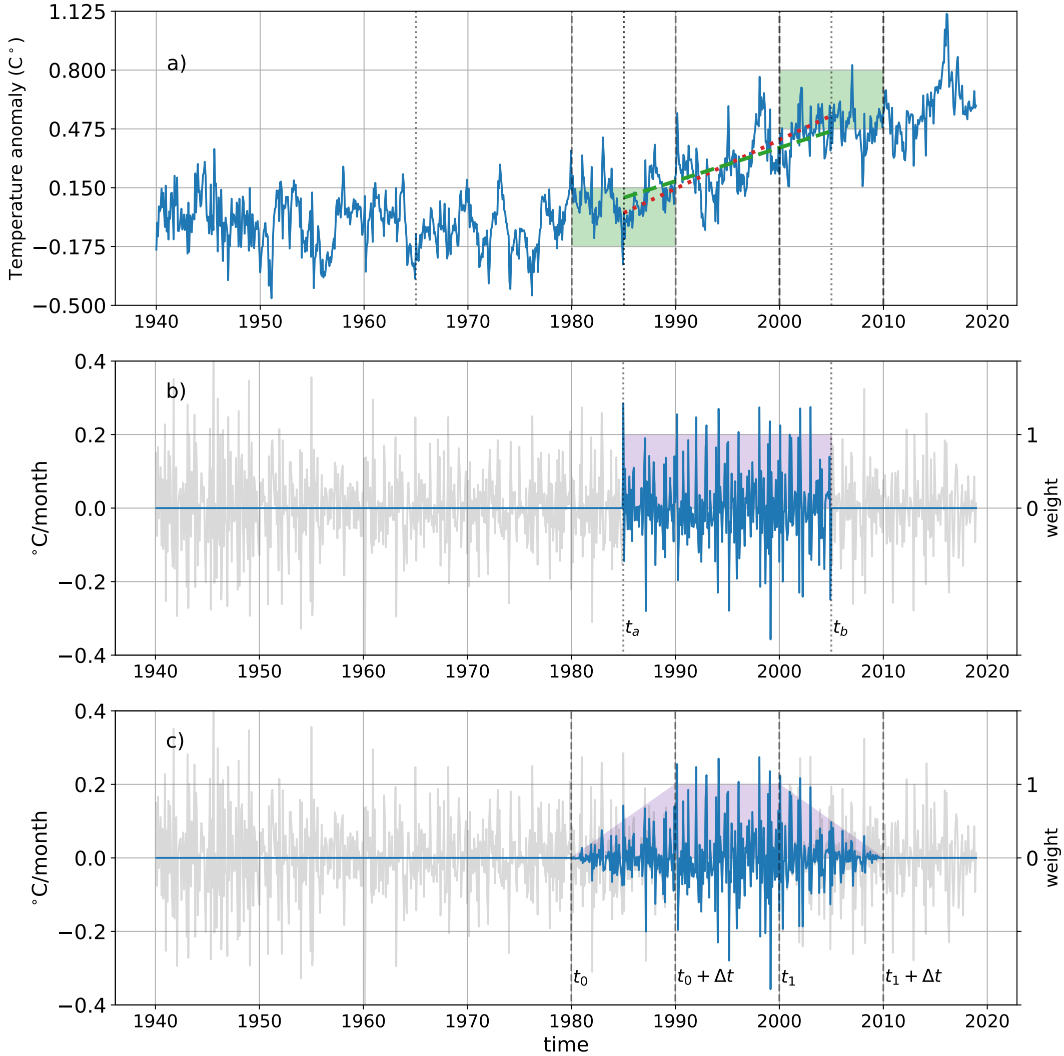


**Figure 1.** Example of the standard boxcar time average compared to the hat average of a time varying quantity. Here, we consider the monthly and globally averaged sea surface temperature anomaly based on the CRUTEM4 and HadSST3 dataset described in Kennedy et al. (2011). a) The snapshot difference (red dotted line) and epoch difference (green dashed line) describe temporal changes in the variable (blue line) differently. The epoch difference is the difference in the boxcar average over the two epochs shown with green rectangles, while the snapshot difference is the difference at the centre of the two epochs, and is therefore sensitive to high-frequency "weather" variability. b) Tendency of temperature with boxcar-averaged weighting (indicated by the blue curve and light purple rectangle). c) the same tendency shown with the hat average weighting (indicated by the blue curve and light purple 'hat' shape). The boxcar average of the tendency relates to the snapshot difference while the hat average relates to the epoch difference. Note that the hat-averaged tendency requires computing linear weighted averages over each epoch period, and boxcar averages between the epochs.

https://doi.org/10.5194/egusphere-2026-3672
Preprint. Discussion started: 22 July 2026


where $*$ denotes convolution, $t'$ is a dummy variable and $w(t)$ is a window function of unit area, which is a symmetric function centred at $t=0$ that is non-zero over some time interval.

The standard boxcar averaging method for diagnostics is equivalent to a convolution with a rectangular window function of unit area and width $\tau = t_1 - t_0$ (shown in Fig. 2a), given by

$$w_{rect}(t;\tau) = \begin{cases} 1/\tau & \text{for } |t| < \tau/2 \\ 0 & \text{elsewhere.} \end{cases} \tag{11}$$

For example, using $w_{rect}$ and its symmetry, and for brevity the notation $\xi' = \frac{\partial \xi}{\partial t}$ for the tendency, equation (2) can be written as the convolution $(\tau w_{rect} * \xi')(t)$ evaluated at the midpoint of the averaging window, $t = t_{rmid} = (t_a + t_b)/2$:

$$\begin{aligned} \xi(\mathbf{x},t_b) - \xi(\mathbf{x},t_a) &= \int_{-\infty}^{\infty} \tau w_{rect}\,(t_{rmid} - t')\,\xi'(t')\,\mathrm{d}t' \\ &= (\tau w_{rect} * \xi')\,(t_{rmid}). \end{aligned} \tag{12}$$

Similarly, a hat average with slope widths of $\Delta t$ and width $\tau$ between the midpoints of the slopes (shown in Fig. 2b) is equivalent to using a trapezoidal window function, $w_{trap}$, given by

$$w_{trap}(t;\tau,\Delta t) = \begin{cases} (t+\tau/2+\Delta t/2)/(\tau\Delta t) & \text{for } -\tau/2-\Delta t/2 < t < -\tau/2+\Delta t/2 \\ (-t+\tau/2+\Delta t/2)/(\tau\Delta t) & \text{for } \tau/2-\Delta t/2 < t < \tau/2+\Delta t/2 \\ 1/\tau & \text{for } -\tau/2+\Delta t/2 < t < \tau/2-\Delta t/2 \\ 0 & \text{elsewhere.} \end{cases} \tag{13}$$

Using $w_{trap}$ and its symmetry, equation (9) can be written as the convolution $(\tau w_{trap} * \xi')(t)$ evaluated at the midpoint of the averaging window, $t = t_{mid} = (t_0 + t_1 + \Delta t)/2$:

$$\begin{aligned} \overline{\xi}_{t_1,t_1+\Delta t} - \overline{\xi}_{t_0,t_0+\Delta t} &= \int_{-\infty}^{\infty} \tau w_{trap}\,(t_{mid} - t')\,\xi'(t')\,\mathrm{d}t' \\ &= (\tau w_{trap} * \xi')\,(t_{mid}). \end{aligned} \tag{14}$$

Noting that $\tau w'_{trap}(t;\tau,\Delta t) = w_{rect}(t+\tau/2;\Delta t) - w_{rect}(t-\tau/2;\Delta t)$, equation (9) can be obtained from the derivative theorem for convolutions, which states $w_{trap} * \xi' = w'_{trap} * \xi$, so it follows that $\tau w_{trap} * \xi' = w_{rect}(t;\Delta t) * \xi(t-\tau/2) - w_{rect}(t;\Delta t) * \xi(t+\tau/2)$, which becomes equation (14) at $t = t_{mid}$.

Note that $w_{trap}$ itself can be expressed as the convolution of two rectangular window functions of widths $\tau$ and $\Delta t$ as $w_{rect}(t;\tau) * w_{rect}(t;\Delta t)$. The special case of a convolution of two equal width rectangular functions ($\tau = \Delta t$) produces a triangular window function, $w_{tri}$ (shown in Fig. 2c), which relates to the epoch difference between two adjacent epochs.

Convolution with a window function $w_{rect}$ or $w_{trap}$ produces a smoothed version of a timeseries. The impact of window functions on the frequency content of a time-averaged budget tendency diagnostic $f(t)$ can be understood using the convolution

https://doi.org/10.5194/egusphere-2026-3672
Preprint. Discussion started: 22 July 2026


theorem for the Fourier transform, $\mathfrak{F}$, given by

$$\mathfrak{F}\{w(t) * f(t)\} = \mathfrak{F}\{w(t)\} \cdot \mathfrak{F}\{f(t)\} = W(\omega) \cdot F(\omega), \tag{15}$$

where $W(\omega)$ and $F(\omega)$ are the Fourier transforms of $w(t)$ and $f(t)$, respectively, and $\omega$ is frequency. The convolution theorem states that time-averaging a model diagnostic multiplies its spectrum by the Fourier transform of the window function used. The extent to which time averaging affects the resolved frequencies of the spectrum of the timeseries therefore depends on the choice of window function. The Fourier transform of the rectangular window function $w_{rect}(t;\tau)$ is given by

$$W_{rect}(\omega;\tau) = \mathrm{sinc}(\omega\tau) = \begin{cases} 1 & \text{for } \omega\tau = 0 \\ \frac{\sin(\pi\omega\tau)}{\pi\omega\tau} & \text{otherwise,} \end{cases} \tag{16}$$

while it follows from the convolution theorem that the Fourier transform of the trapezoidal window function $w_{trap}(t;\tau,\Delta t) = w_{rect}(t;\tau) * w_{rect}(t;\Delta t)$ is given by

$$W_{trap}(\omega;\tau,\Delta t) = \mathrm{sinc}(\omega\tau)\mathrm{sinc}(\omega\Delta t) = \frac{\sin(\pi\omega\tau)\sin(\pi\omega\Delta t)}{\pi^2\omega^2\tau\Delta t}. \tag{17}$$

The Fourier transforms of these window functions are shown in Fig. 2f.

Creating (say) monthly timeseries involves sampling at a monthly period, which cannot correctly represent frequencies higher than the Nyquist frequency of 0.5 cycles per month. Instead, any variability at higher frequency is aliased, contaminating the resolved variability below the Nyquist frequency. Saving monthly averages (rather than snapshots) reduces this aliasing because the Fourier spectrum of the raw data is multiplied by $W_{rect}(\omega;\tau)$ with $\tau = 1\,\mathrm{mo}$, which has significantly reduced amplitude at the Nyquist frequency and above (frequencies exceeding 0.5 in magnitude on the scale of Fig. 2f), falling off as $\omega^{-1}$ at large frequencies. However, aliasing is reduced even more effectively when using the trapezoidal filter $W_{trap}(\omega;\tau,\Delta t)$, which scales as $\omega^{-2}$ at large frequencies.

Fig. 2 illustrates the effect of these filtering methods on the globally-averaged sea surface temperature tendency shown in Fig. 1b. The standard moving average (blue curve in Fig. 2d) exhibits substantial high-frequency variability compared to the moving averages computed using $w_{trap}$ and $w_{tri}$. By Eq. (12), this moving average corresponds to an unfiltered moving difference of the underlying variable $\xi$, which contains substantial variability at frequencies beyond the Nyquist limit. Aliasing spreads the energy associated with these unfiltered high frequencies into the resolved frequencies. This aliasing is part of the reason the spectrum decays so much more slowly with boxcar filtering than the other methods in Fig. 2e.

The trapezoidal moving average (orange curve in Fig. 2d) is substantially smoother than the boxcar average of the tendency, which is expected since averaging with $w_{trap} = w_{rect}(t;\tau) * w_{rect}(t;\Delta t)$ is equivalent to convolving the time series with two rectangular window functions (i.e. the orange curve is the blue curve after a second smoothing by $w_{rect}(t;\Delta t)$). By Eq. (14), a moving epoch difference equates to a trapezoidal moving average of the tendency $\xi'(t)$, which is equivalent to convolving $\xi(t)$ with $w_{rect}(t;\Delta t)$ before differencing (compare equations (17) and (16)), reducing the power of the high-frequency components by a factor of about $10^8$ (note the log scale in Fig. 2e), or the amplitude by a factor of $10^4$.

https://doi.org/10.5194/egusphere-2026-3672
Preprint. Discussion started: 22 July 2026


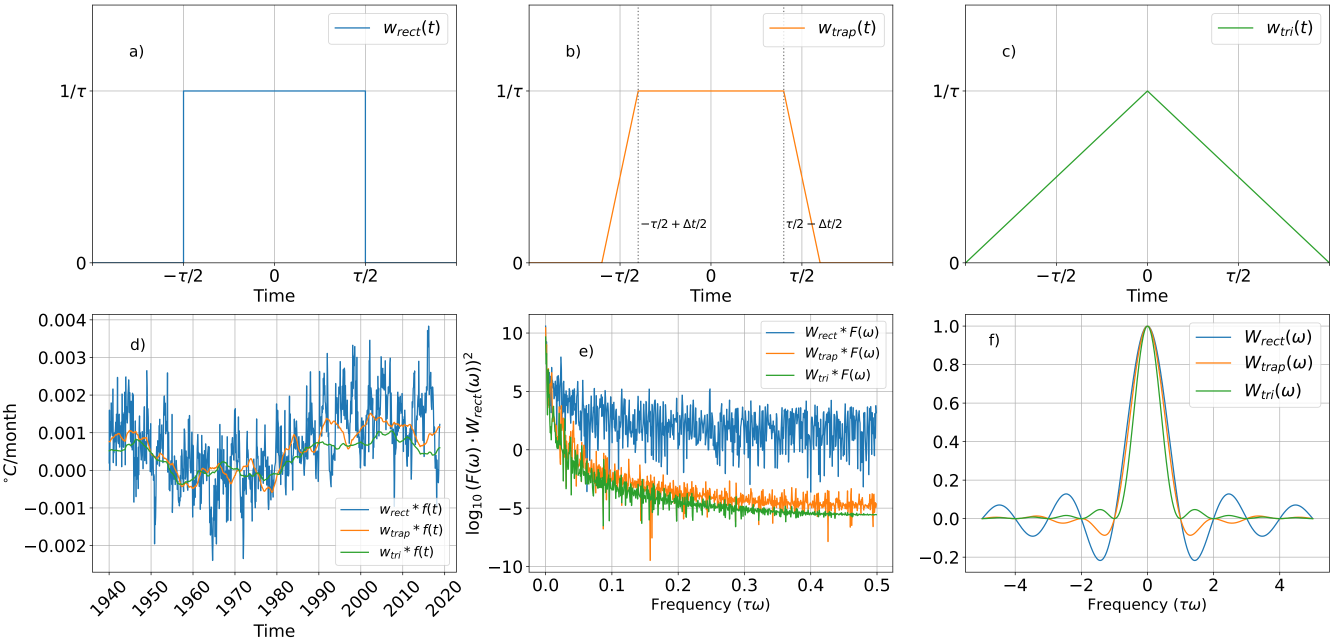


**Figure 2.** Window functions for the a) rectangular (boxcar) window $w_{rect}$, b) trapezoidal window $w_{trap}$, c) triangular window $w_{tri}$. d) Moving average of the monthly SST tendency time series (shown in Fig. 1b) under convolution with the boxcar (blue), trapezoidal (orange), and triangular (green) window functions for $\tau = 20$ years and $\Delta t = 5$ years. e) Power spectrum of d) in the frequency domain. f) Fourier transforms of the boxcar, trapezoidal and triangular window functions.

## 3 Ocean model and heat content diagnostics

To demonstrate the utility of the hat average, we apply hat-averaging to the heat budget of the ACCESS-OM2 1-degree global ocean sea-ice model (Kiss et al., 2020) to analyze the drivers of heat content change over the late twentieth and early twenty-first centuries. ACCESS-OM2 comprises Version 5.1 of the Modular Ocean Model (MOM5.1, Griffies, 2012) coupled to the CICE sea ice model (version 5.1.2, Hunke et al., 2015). The simulation was initialised from the WOA13 temperature and salinity analysis (Locarnini et al., 2013; Zweng et al., 2013) and cycled three times over a 61 year period from 1958-2018 using the JRA55-do forcing dataset (Tsujino et al., 2018), following the OMIP-2 protocol (Griffies et al., 2016; Tsujino et al., 2020).

The heat budget of an ACCESS-OM2 model grid cell is given by,

$$\partial_t(\rho_0 C_p \Theta \Delta z) = \rho_0 C_p \left[ \underbrace{-\nabla_z \cdot (\Delta z\, \mathbf{u}\Theta) - \delta_k(w\Theta)}_{A} \underbrace{-\delta_k F^z}_{V} + \underbrace{\nabla_z \cdot (\Delta z\, \mathbf{K}\nabla\Theta)}_{N} \right] + Q, \tag{18}$$

where $\Delta z$ is the time and space dependent thickness of each model grid cell (MOM5 uses $z^*$ generalised vertical coordinates), $\mathbf{u}$ is the horizontal velocity, $w$ is the vertical velocity, $\Theta$ is the Conservative Temperature (McDougall, 2003; McDougall and Barker, 2011), $\boldsymbol{K}$ is the symmetric neutral diffusion tensor, $C_p = 3989.245$ J kg$^{-1}$ K$^{-1}$ is the specific heat capacity, and

https://doi.org/10.5194/egusphere-2026-3672
Preprint. Discussion started: 22 July 2026


$\rho_0 = 1035$ kg m$^{-3}$ is the Boussinesq reference density. Due to being multiplied by $\rho_0\, C_p$, each term in equation (18) has units of W m$^{-2}$, corresponding to the heat content tendency per unit horizontal area within each grid cell.

The first term on the right hand side, $A$, denotes convergence of advective fluxes, comprised of horizontal and vertical advective fluxes. Note that the cell integrated vertical flux convergence reduces to the difference in vertical advective fluxes across the upper and lower cell interfaces, here written as the discrete difference $-\delta_k(w\,\Theta) = -[(w\,\Theta)_{\text{k-top}} - (w\,\Theta)_{\text{k-low}}]$. For our analysis we also include parameterised mesoscale and submesoscale eddy stirring in $A$, which are parameterised using a skew diffusive approach in ACCESS-OM2 (Gent and McWilliams, 1990; Gent et al., 1995; Griffies, 1998; Fox-Kemper et al., 2008). The second term, $V$, denotes the cell integrated vertical convergence of subgrid mixing fluxes $F^z$, parameterized in ACCESS-OM2 using the K-profile parameterization (KPP) for the surface boundary layer (Large et al., 1994); a bottom-intensified internal tidal mixing scheme (Simmons et al., 2004); vertical convective adjustment realized by enhancing the vertical diffusivity (Klinger et al., 1996); a fixed background diffusivity following Jochum (2009); plus the vertical diagonal portion of the neutral diffusion (Griffies et al., 1998; Redi, 1982). $N$ contains the remaining portion of the parameterised neutral diffusion, and $Q$ denotes surface thermal forcing. Both boxcar-averaged and rising weighted averages of these heat budget diagnostics were computed online and output monthly over the duration of the last cycle of the ACCESS-OM2 simulation. Details of the numerical implementation of the hat-average in ACCESS-OM2 are described in Appendix B.

We chose the period between 1990 and 2010 of the third cycle of the ACCESS-OM2 1-degree global ocean simulation to demonstrate the benefit of hat-averaged model diagnostics for climate scale variability (see Kiss et al., 2020, Fig. 3a). This period exhibits a moderate long-term warming trend (the change in "climate"). Furthermore, a moderate El Niño event is active in 2010 introducing some interannual variability. We computed the epoch difference using a ten year epoch period, with the final epoch from 2005 to 2015 and the initial epoch from 1985 to 1995. This choice of epoch length is consistent with that used by Deser et al. (2012). In contrast, the snapshot difference between midpoints of this epoch on the 1st January 2010 and 1st January 1990 is strongly affected by the moderate El Niño event in 2010 and shows a weaker trend.

To demonstrate the effect of the different time-averaging methods, we consider the change in the heat content per unit volume as vertically integrated from a model depth surface at nominal depth $D > 0$ to the sea surface $\eta$

$$H_D(x,y,t) = \int\limits_{-D}^{\eta(x,y,t)} \rho_0\, C_p\, \Theta(x,y,z,t)\, \mathrm{d}z, \tag{19}$$

with $H_D$ having units of J m$^{-2}$. Note that we consider the top 100m ($H_{100}$) below, with it being understood that the integration is performed over complete model grid cells and not strictly the top 100m. Additionally, we examine changes in the heat content as a function of depth as integrated horizontally over the globe.

$$H_Z(z,t) = \frac{1}{\Delta Z} \iint \rho_0\, C_p\, \Theta(x,y,z,t)\, \Delta z(x,y,z,t)\, \mathrm{d}x\, \mathrm{d}y, \tag{20}$$

where $\Delta Z = \iint \Delta z(x,y,z,t)\, \mathrm{d}x\, \mathrm{d}y / \iint \mathrm{d}x\, \mathrm{d}y$ is the nominal grid cell thickness used to convert $H_Z$ to units of J m$^{-1}$.

https://doi.org/10.5194/egusphere-2026-3672
Preprint. Discussion started: 22 July 2026


Integrating the heat budget (Eq. (18)) horizontally over the globe (so that horizontal fluxes disappear) quantifies the processes that contribute to the vertical profile of heating in the ocean (Griffies et al., 2015), given by

$$\frac{\partial}{\partial t}(H_Z\,\Delta Z) = \underbrace{-\rho_0 C_p \iint \delta_k(w\,\Theta)\mathrm{d}x\,\mathrm{d}y}_{A_Z} \; \underbrace{-\rho_0 C_p \iint \delta_k F^z \mathrm{d}x\,\mathrm{d}y}_{V_Z}$$
$$\underbrace{-\rho_0 C_p \iint \delta_k(\boldsymbol{K}\,\nabla\Theta)\cdot\hat{\mathbf{k}}\mathrm{d}x\,\mathrm{d}y}_{N_Z} \; + \; \underbrace{\rho_0 C_p \iint Q \mathrm{d}x\,\mathrm{d}y}_{Q_Z} \tag{21}$$

where the units are Watts (we note that the right hand side is thickness weighted on the model timestep). Eq. (21) describes the balance between surface forcing, $Q_Z$, and vertical advection and mixing within the ocean. The mixing is divided into parameterized vertical mixing $V_Z$ and the vertical component of neutral diffusion, $N_Z$, while vertical advection, $A_Z$, contains both resolved advection and parameterised eddy advection and the vertical heat flux from turbulent mixing (Griffies et al., 2015; Holmes et al., 2022). Horizontal heat advection is negligible in the horizontal integral, since runoff does not carry heat through the lateral boundary of this model, and the model maintains near-constant volume over long timescales.

## 4 Results

Fig. 3a shows the epoch difference of $H_D$ over the trend period and over the top 100m, $\overline{H}_{100}(2015;2005) - \overline{H}_{100}(1995;1985)$, while Fig. 3b shows the equivalent snapshot difference between 1 January 2010 and 1 January 1990. The epoch difference clearly smooths the transient features associated with weather events and interannual variability that strongly impact the snapshot difference. In particular, the snapshot difference is strongly affected by the presence of an El Niño event in January 2010. This El Niño event shows warming in the eastern equatorial Pacific and cooling in the western equatorial Pacific associated with the flattening of the equatorial Pacific thermocline. As a further demonstration, Fig. 3c shows the snapshot difference between 1 January 2014 and 1 January 1998, highlighting the impact of the extreme 1998 El Niño (with an opposite signed dipole in the equatorial Pacific as the El Niño is at the beginning of the period). These snapshot differences are not representative of the long-term change in upper 100m heat content. In contrast, the epoch difference reveals the smooth regional background trend in upper 100m heat content, with warming in the western Pacific, North Atlantic and at the boundary of the Atlantic and Southern oceans and cooling in the eastern Pacific, which may be associated with the transition from the warm to cool phase of the Interdecadal Pacific Oscillation during this period (Dong and Dai, 2015).

The horizontally integrated heat content change reveals the vertical structure of the heat content change (shown for the upper 800 m in Fig. 3d). The epoch difference over the trend period, $\overline{H}_Z(2015;2005) - \overline{H}_Z(1995;1985)$ (shown in the blue curve in Fig. 3d) is non-negative over the entire water column, which reflects the accumulation of heat in the interior ocean due to increased radiative forcing over the period 1990 to 2010. The snapshot difference between 1 January 2010 and 1 January 1990 (orange curve in Fig. 3d) reveals the impact of the high-frequency variability on heat content change, with a warming anomaly over the upper 100 m and a cooling anomaly between 100 m and 300 m associated with the flattening of the thermocline during the 2010 El Niño (e.g. Roemmich and Gilson, 2011; Holmes et al., 2022). This dipole of upper ocean heat content change is

https://doi.org/10.5194/egusphere-2026-3672
Preprint. Discussion started: 22 July 2026


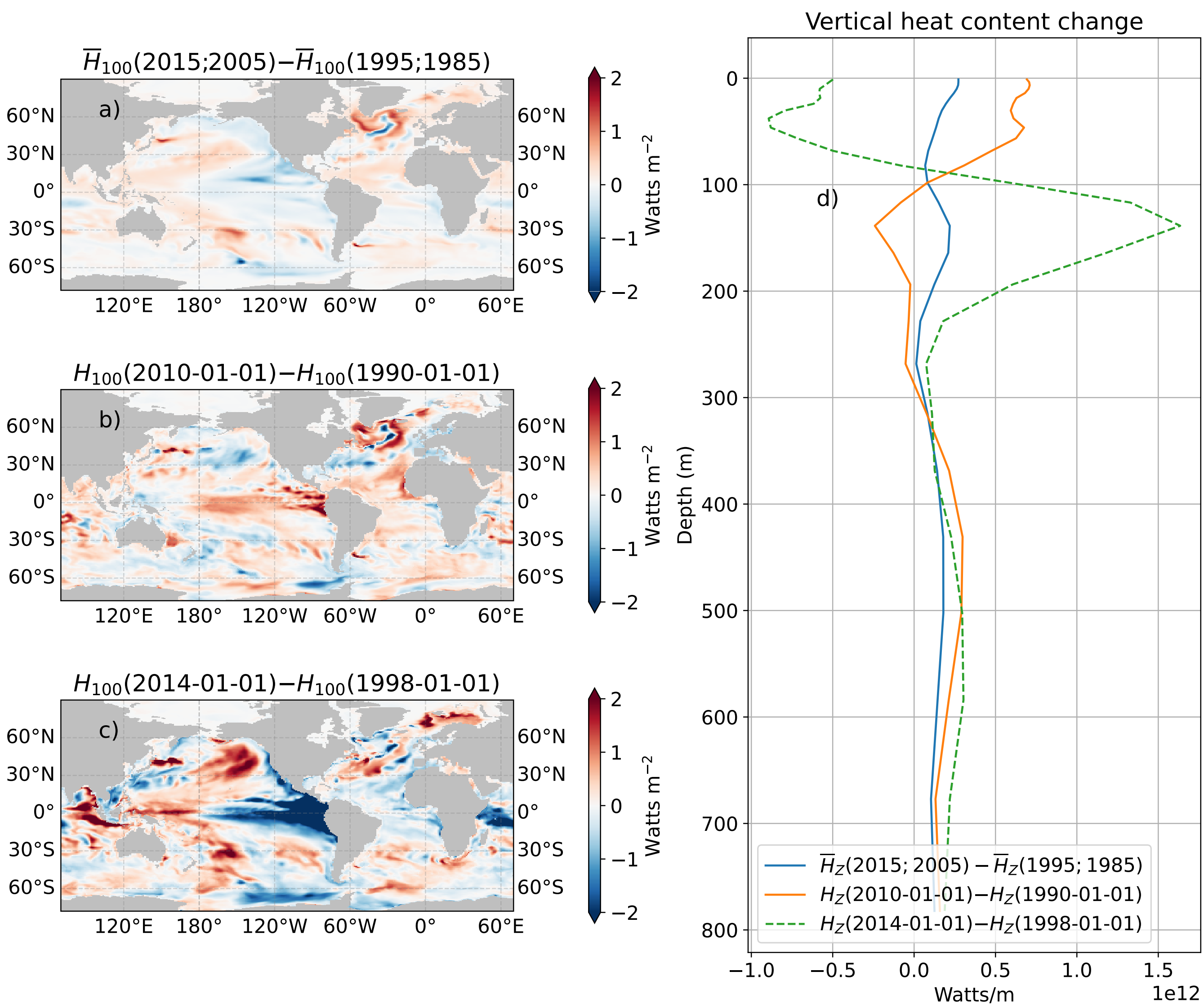


**Figure 3.** The spatial pattern and vertical profile of heat content change (divided by elapsed time) in the third cycle of the inter-annually forced ACCESS-OM2 simulation. a) Epoch difference of upper 100m ocean heat content $\overline{H}_{100}(2015;2005) - \overline{H}_{100}(1995;1985)$, divided by the elapsed time between the midpoints of the two epochs. b) Snapshot difference (divided by elapsed time) over the equivalent period $H_{100}(2010\text{-}01\text{-}01) - H_{100}(1990\text{-}01\text{-}01)$ showing small scale transient features and upper ocean warming from the moderate El Niño in 2010 in the eastern Pacific. c) An alternate snapshot difference between 2014 and 1998, $H_{100}(2014\text{-}01\text{-}01) - H_{100}(1998\text{-}01\text{-}01)$, showing the impact of a strong El Niño event in 1998. d) The vertical profile of globally-integrated heat content changes showing both the epoch difference in blue and snapshot difference in orange for the trend period. The dashed green curve shows the vertical profile over the same period as c).

https://doi.org/10.5194/egusphere-2026-3672
Preprint. Discussion started: 22 July 2026


further highlighted by the vertical structure of the snapshot difference between 1 January 2014 and 1 January 1998 (dashed green curve in Fig. 3d), emphasizing the extreme 1998 El Niño event.

### 4.1 Process contributions to heat content change

The contrast between epoch and snapshot differences illustrated in the previous section is not surprising. These techniques are widely used in climate science. However, what this difference means for analyses of the processes that drive these changes (i.e. the heat budget) is more subtle, as we now illustrate.

We begin by examining the horizontally integrated heat budget (Eq. (21)) under both hat-averaging, weighted over the 10 year epochs 01-01-1985 to 01-01-1995 and 01-01-2005 to 01-01-2015, and standard boxcar-averaging, between 1 January 2010 and 1 January 1990 (shown in Fig. 4, where we have divided each term by the mean grid cell thickness). All processes are dominated by a long-term mean balance irrespective of the time-averaging method. For example, the surface forcing term, $Q_Z$, is dominated by shortwave heat penetration between the surface and a depth of about 20 m, which is balanced by strong vertical mixing (Fig. 4 c). Below the surface, vertical advection and mixing transport the surface heat downward. Here, vertical advection includes the contribution from parameterised eddies, which have been shown to partially balance downward heat transport (Gregory, 2000; Griffies et al., 2015).

Fig. 4 highlights a difficulty in attributing changes in ocean heat content to particular processes in the presence of large compensating balances between terms. As the flux convergences that contribute to the mean balance in Eq. (21) are much larger than the total tendency, the difference between hat-averaging and boxcar time-averaging of the budget is small relative to the budget terms themselves. Only a small difference is visible between $\widehat{A}_Z$ and $\overline{A}_Z$ in Fig. 4a and Fig. 4b, while no difference is visible in the mixing terms between the two time-averaging methods.

To address this issue, we consider the budget for a property, $\xi$, given by Eq. (1). The boxcar time-average of each process, $f_i$, can be decomposed into a component associated with a long-term budget balance, $f_i^{\overline{C}}$, and an anomaly in each process, $\overline{f}_i^A$,

$$\frac{1}{\Delta t}(\xi(t_b) - \xi(t_a)) = \sum_{i=1}^{n} \overline{f}_i = \sum_{i=1}^{n} (\overline{f}_i^A + f_i^{\overline{C}}). \tag{22}$$

The overline on the superscript in the control term, $f_i^{\overline{C}}$, denotes a standard boxcar average computed over the "control", or "climatology", period (a different averaging period to $\overline{f}_i$). In the ACCESS-OM2 heat content example, for the control period we use a period starting 5 years before the end of the second cycle and ending 5 years before the end of the third cycle. The choice of a full cycle ensures that this boxcar average is not overly affected by high-frequency variability, as the ocean model experiences forcing from the same atmospheric state at the start and end of the period in each cycle. The choice of starting/ending 5 years before the end of the cycles is made in order to compare with the hat-averaged budget as described next.

https://doi.org/10.5194/egusphere-2026-3672
Preprint. Discussion started: 22 July 2026


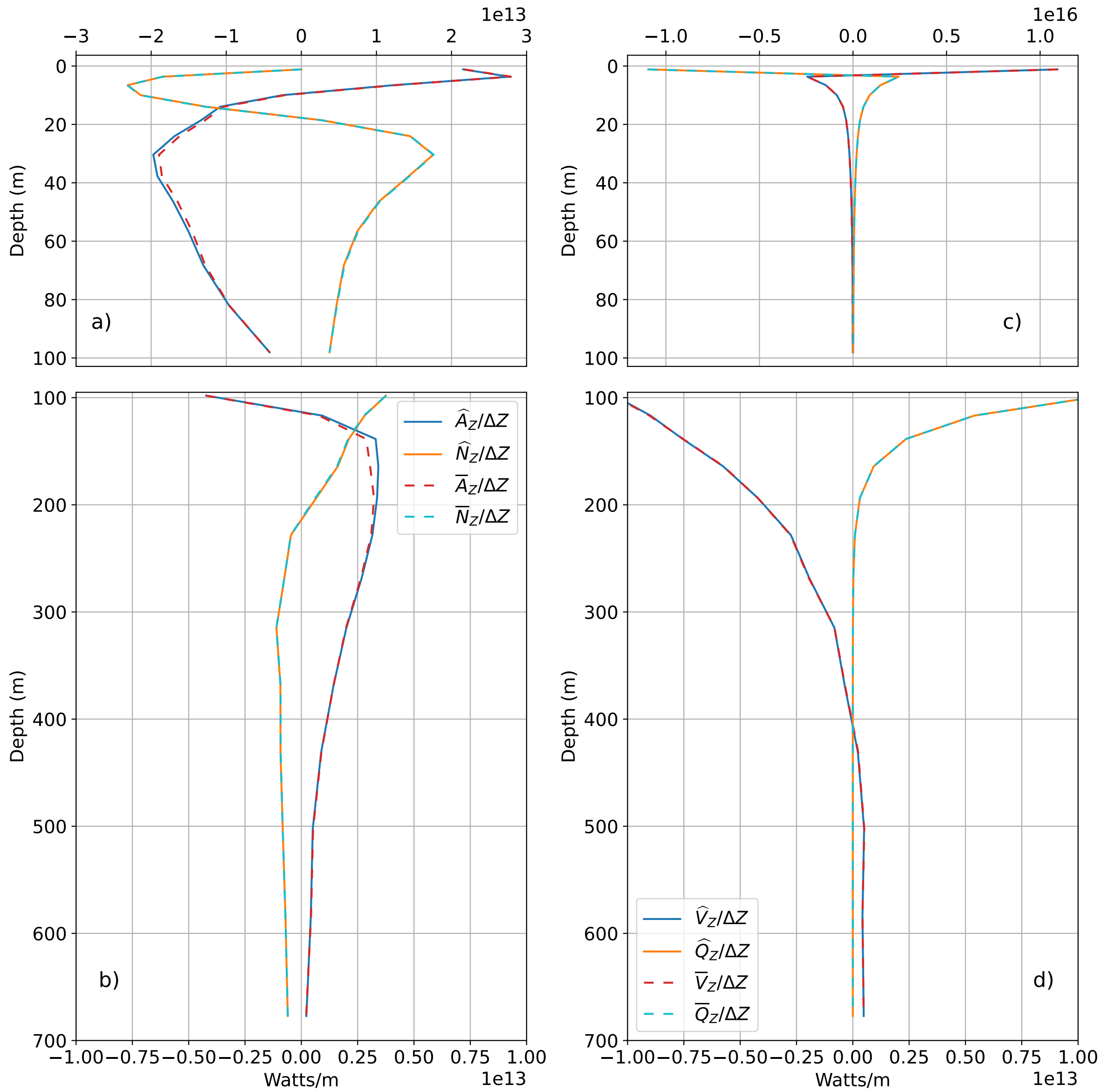


**Figure 4.** Depth profiles of the terms of the horizontally integrated heat budget over the full ocean depth (Eq. (21)) under the two averaging methods, with the hat-averaging period weighted over the 10 year epochs 01-01-1985 to 01-01-1995 and 01-01-2005 to 01-01-2015, and the boxcar average taken between 01-01-1990 to 01-01-2010. The hat-averaged flux convergences of advection ($\widehat{A}_Z$, blue curve) and neutral diffusion ($\widehat{N}_Z$, orange curve) and equivalent boxcar-averaged $\overline{A}_Z$ (dashed red curve) and $\overline{N}_Z$ (dashed cyan curve) shown between 0m-100m depth in a) and between 100m-700m in b) (shown in units Watts/m). The convergence of surface fluxes and vertical mixing for $\widehat{Q}_Z$ (orange curve) and $\widehat{V}_Z$ (blue curve) with hat averaging, and $\overline{Q}_Z$ (dashed cyan curve) and $\overline{V}_Z$ (red dashed curve) with boxcar averaging are shown between 0m-100m in c) and between 100m and 700m in d).

https://doi.org/10.5194/egusphere-2026-3672
Preprint. Discussion started: 22 July 2026


A similar approach can be applied to the hat-average diagnostics to isolate the processes contributing to the epoch difference, given by

$$\frac{1}{\Delta t}(\overline{\xi}(t_1+\Delta t;t_1)-\overline{\xi}(t_0+\Delta t;t_0))=\sum_{i=1}^{n}\widehat{f}_i=\sum_{i=1}^{n}(\widehat{f}_i^A+f_i^{\widehat{C}}). \tag{23}$$

Here, once again the hat symbol on the superscript in the control term, $f_i^{\widehat{C}}$, denotes a hat average computed over the control period - a different averaging period to $\widehat{f}_i$, For this “control” period in the ACCESS-OM2 heat content example, we use a difference in 10 year epochs, with the initial epoch as the final ten years of the second cycle and the final epoch as the final ten years of the third cycle. This epoch period was chosen so that the boxcar average of the control is taken between the midpoints of the epochs.

### 4.2 Application to upper 100m heat content

We now apply the mean/anomaly balance decomposition described in the previous section to the specific example of the upper 100m heat content of ACCESS-OM2. Figs. 5a-5c show the hat average of the spatial pattern of budget processes over the upper 100 m in the Pacific Ocean computed over epochs 01-01-1985 to 01-01-1995 and 01-01-2005 to 01-01-2015, while Figs. 5d-5f show the corresponding boxcar averages, computed between between 1 January 2010 and 1 January 1990. Here we have combined surface fluxes and vertical mixing in Figs. 5a and 5d, and advection and neutral diffusion in Figs. 5b and 5e.

While the subtraction of the long-term mean control budget balance reduces the degree of cancellation between processes, the total heat content change (Figs. 5c and 5f) is still substantially smaller than the individual process contributions. Despite this cancellation between the processes, there is a substantial difference in the budget terms under the two time-averaging methods. This difference is most evident in the eastern equatorial region near 120W where the magnitude of the sum of the surface forcing and vertical mixing is smaller under hat time-averaging than boxcar-averaging (compare Figs. 5a and Fig. 5d). The difference between hat-averaging and boxcar-averaging is even larger for the combined advection and neutral diffusion terms than the surface forcing and vertical mixing terms (compare Figs. 5b and Fig. 5e). This result suggests that the heat anomaly throughout most of the central and eastern equatorial Pacific highlighted by the snapshot difference (Fig. 5f) is driven largely by advection and neutral diffusion, with some significant compensation by surface fluxes and vertical mixing. This is consistent with the vertical heaving of the equatorial Pacific thermocline that occurs during El Niño events. However, this vertical heaving is not relevant for the long-term trend in heat content; it is instead associated with high-frequency variability. This high-frequency advective process is smoothed out when analysing the epoch difference (Fig. 5c) and its process contributions using hat averaging.

### 4.3 Application to horizontally-integrated heat content

A hat-averaged budget of the anomalous tendency in the horizontally integrated budget (Eq. (21)) can be computed by subtracting the hat-averaged control budget from the hat-averaged budget over the trend period, given by

$$\frac{\Delta Z}{\Delta t}(\overline{H}_Z(2015;2005)-\overline{H}_Z(1995;1985))^A=\widehat{\partial_t H_Z}^A=\widehat{A}_Z^A+\widehat{N}_Z^A+\widehat{V}_Z^A+\widehat{Q}_Z^A, \tag{24}$$

https://doi.org/10.5194/egusphere-2026-3672
Preprint. Discussion started: 22 July 2026


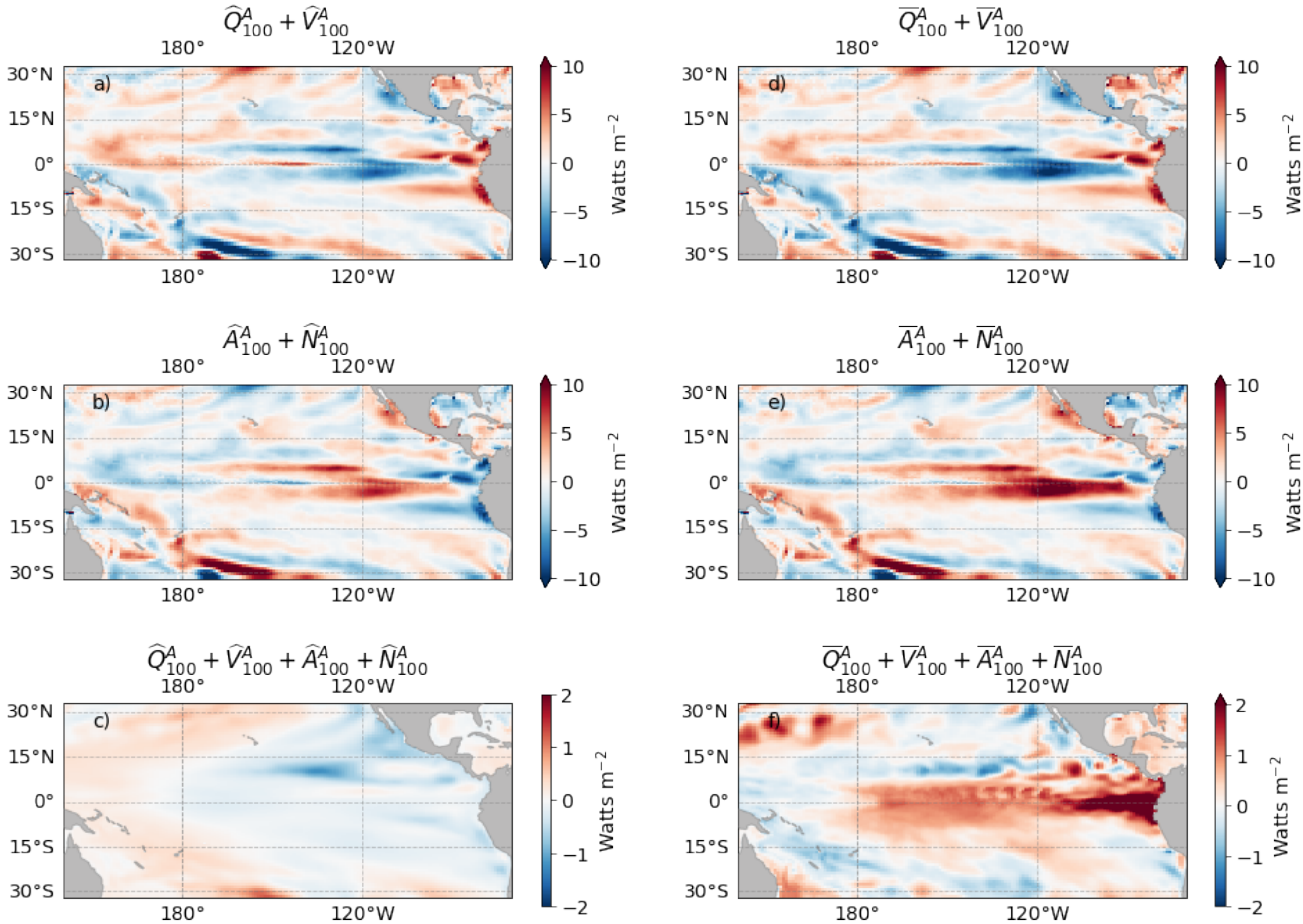


**Figure 5.** Surface forcing and vertical mixing compared to advection and neutral mixing in the upper 100 m (denoted by the subscript for integration above a model depth level of approximately 100 m as in Eq. (19)) of the Equatorial Pacific of ACCESS-OM2 under the two time-averaging methods, with the long-term average control removed (denoted by superscript $A$). Hat averages of the a) anomalous surface forcing plus vertical mixing $\widehat{Q}^A_{100}+\widehat{V}^A_{100}$, b) advection plus neutral diffusion $\widehat{A}^A_{100}+\widehat{N}^A_{100}$, c) total tendency. Boxcar averages of the d) surface forcing plus vertical mixing $\overline{Q}^A_{100}+\overline{V}^A_{100}$ and e) advection plus neutral diffusion $\overline{A}^A_{100}+\overline{N}^A_{100}$. f) boxcar-averaged total tendency. The time periods considered are the same as in Figs. 4a and 4b - corresponding to the epoch difference between 2005-2015 and 1985-1998 (for panels a-c) and the snapshot difference between 2010-01-01 and 1990-01-01 in panels d-f.

https://doi.org/10.5194/egusphere-2026-3672
Preprint. Discussion started: 22 July 2026


where $\Delta t$ is 20 years (the elapsed time between the midpoints of the epochs). Similarly, the boxcar-averaged budget of the anomaly is computed by subtracting the respective terms of the boxcar-averaged control budget from the boxcar average over the trend period of interest, given by

$$\frac{\Delta Z}{\Delta t}(H_Z(2010\text{-}01\text{-}01) - H_Z(1990\text{-}01\text{-}01))^A = \overline{\partial_t H_Z}^A = \overline{A}_Z^A + \overline{N}_Z^A + \overline{V}_Z^A + \overline{Q}_Z^A, \tag{25}$$

where $\Delta t$ is 20 years (the elapsed time between the snapshots).

The vertical profiles of the hat-averaged and boxcar-averaged budget processes (blue and orange, respectively, in Fig. 6) reveal larger differences from interannual variability than for the upper 100m heat content example considered in the previous subsection. The warming anomaly that is present in the upper 100 m of the total tendency anomaly under boxcar time-averaging, $\overline{\partial_t H_Z}^A$ (orange line in Fig. 6d), occurs through a combination of positive anomalous surface fluxes (in the upper few meters), vertical mixing (above 25m), upward heave from advection (20-60m) and neutral diffusion (60-100m). Under hat averaging (i.e. the epoch difference) this upper 100m warming anomaly is largely absent (compare blue and orange lines in Fig. 6d). Below the upper $\sim$ 20m (where the contribution of surface forcing is weak), the difference between hat averaging and boxcar averaging is largely attributable to the advection, as neutral diffusion is similar and vertical mixing differences are of the wrong sign acting to compensate for the advection-driven differences. Below 100m the cooling evident in the snapshot difference is also driven by advection, consistent with vertical heaving leading to a cooling below 100m and a warming above 100m, as expected during a flattening of the thermocline in the equatorial Pacific during El Niño events. The epoch difference instead isolates the longer term changes associated with ocean warming, with advection redistributing excess heat accumulating in the top 100m of the ocean downwards to deeper depths (consistent with Gregory, 2000; Griffies et al., 2015).

## 5 Discussion: When is hat averaging needed?

Climate change is characterised by changes in the long term mean state of the earth system. In this study we have shown that in order to precisely quantify the contribution of individual processes to climate change in numerical climate models, thoughtful treatment of model based tendency terms is required. We have shown that how these terms are time averaged can influence how we interpret their contribution to ocean heat content trends. In this section we explore where the hat average method is important.

To aid this discussion we consider a two-layer model of the climate system consisting of a shallow mixed layer ocean which experiences higher frequency temperature variability, and a deep ocean layer below the mixed layer whose temperature variability is weaker and lower frequency (e.g., Gregory, 2000; Held et al., 2010). This two-layer model is given by

$$C_U \frac{\mathrm{d}T_U}{\mathrm{d}t} = -\beta T_U - \gamma(T_U - T_D) + \mathcal{F}, \tag{26}$$

$$C_D \frac{\mathrm{d}T_D}{\mathrm{d}t} = \gamma(T_U - T_D), \tag{27}$$

where $T_U$ is the temperature of the upper layer and $C_U$ is its heat capacity, $\mathcal{F}$ is the atmospheric forcing, $\beta$ is the coefficient of the upward surface heat flux and $\gamma$ is the coefficient of the heat exchange between the two layers. $T_D$ is the temperature of the

https://doi.org/10.5194/egusphere-2026-3672
Preprint. Discussion started: 22 July 2026


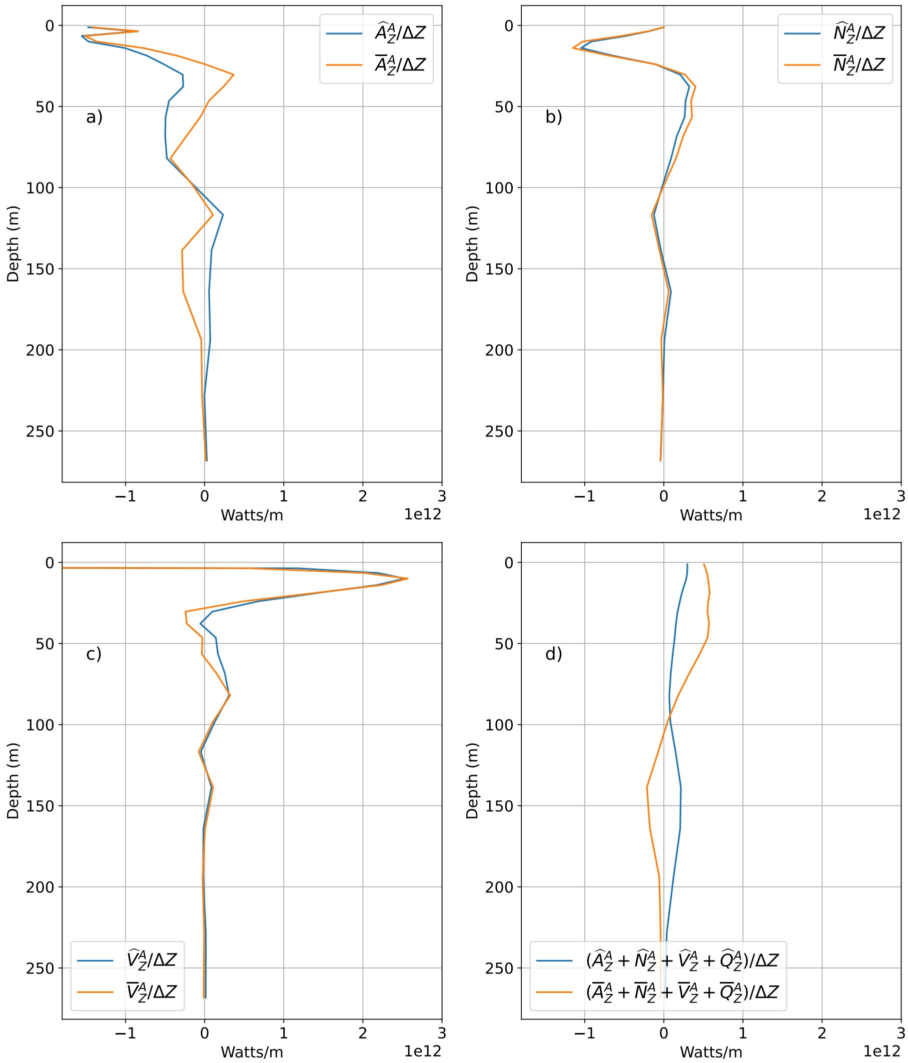


**Figure 6.** Comparison of the horizontally integrated heat budget anomalies in the upper 250m (where the long-term control has been subtracted) of the hat-averaged ($\widehat{\cdot}$) and boxcar-averaged ($\bar{\cdot}$) oceanic processes for the ACCESS-OM2 model. Hat averages are computed with the rising weighted period between 01-01-1985 and 01-01-1995 and falling weighted period between 01-01-2005 and 01-01-2015. Standard boxcar averages computed between 01-01-1990 and 01-01-2010. Comparisons of a) advection ($\widehat{A}_Z^A$ and $\overline{A}_Z^A$), b) neutral diffusion ($\widehat{N}_Z^A$ and $\overline{N}_Z^A$), c) vertical diffusion ($\widehat{V}_Z^A$ and $\overline{V}_Z^A$) and d) total tendency of the anomaly under both averaging methods (including the contribution from surface fluxes, $Q_Z^A$, which is not plotted separately).

https://doi.org/10.5194/egusphere-2026-3672
Preprint. Discussion started: 22 July 2026


deep ocean layer and $C_D$ is the heat capacity of this layer (Eq. (27)). An important assumption is that the surface layer has a significantly smaller heat capacity than the deep layer, $C_U \ll C_D$.

Increased concentration of greenhouse gases perturbs the radiation impacting the ocean surface which leads to an imbalance between the incoming and outgoing fluxes, i.e. an anomaly in $\mathcal{F}$. The small heat capacity of the surface ocean layer means that it quickly warms and adjusts, so that $\mathcal{F}$ will be balanced by the outgoing heat, $\beta T_U + \gamma(T_U - T_D)$. If $\mathcal{F}$ varies over longer time-scales than the relaxation time of the upper ocean layer then the tendency term on the left hand side can be ignored altogether. In this sense, changes in mixed layer temperature (or air temperature) are more appropriately explained by a change in the quasi-equilibrium balance of tendency terms rather than as an integral of the net tendency (e.g. Laliberté et al., 2015).

Unlike the upper ocean, the larger heat capacity of the deep ocean below the mixed layer means that heat storage is not negligible and the tendency term on the left hand side cannot be ignored and, indeed, may be of primary interest. Since, in this simplified model, the transfer of heat is proportional to the difference between the two layers, the deep ocean heat content will fluctuate according to temperature changes in the upper layer. Any perturbation from equilibrium due to changes in $\mathcal{F}$ will result in a nonzero transfer of heat between the layers. This heat transfer will contain components associated with natural variability as well as any component associated with a long-term deviation from equilibrium.

The total change in the tendency terms of Eq. (26) and (27) over any period is given by the accumulation of processes on the right-hand side of each equation. If the period of interest is an integer multiple of modes of variability in $\mathcal{F}$ then the temperature change in the surface layer will be close to zero, and the heat transport between layers will be proportional to the accumulated heat in the deep layer. In practice, however, the modes of variability of $\mathcal{F}$ are rarely integer multiples of the period of interest, so the averaged change in the surface layer will be non-zero, and the energy transfer between the layers will contain a component associated with the natural variability as well as the long term heat-content change.

The two-layer model shows why hat-averaging is needed to quantify process contributions to accumulated heat content changes, particularly when these changes are small relative to natural variability in the system. However, since variability affects the heat transfer between the layers, hat-averaging provides a robust method to quantify the mean contribution of different processes in any system with natural variability. For example, if the long-term change in the lower layer is negligible ($T_D$ is near constant over time), variability in the surface forcing may still affect the heat transport between layers under standard boxcar averaging. If, in addition to variability in the surface forcing, the temperature in the layers is subject to variability (for example, if there are volume changes due to heaving of the interface between the upper and deep layers), additional noise will be present in the heat transfer between the layers under standard averaging. In such cases, temperature changes should be quantified using epoch differences. The hat-averaged budget therefore provides a natural method to quantify the contributions of different processes when a system is subject to high-frequency variability.

## 6 Conclusions

We have presented a time-averaging method, the *hat-average*, which relates tendencies of a property to the property's long-term change characterised by an epoch difference. As well as yielding an exact relationship between property change and

https://doi.org/10.5194/egusphere-2026-3672
Preprint. Discussion started: 22 July 2026


processes of interest, the hat average filters out noise from high-frequency variability that affects conventional time-averaging of budget tendencies. The hat-averaged budget is easily implemented in simulations as linearly weighted integrals, which can be combined to relate the budget to epoch differences of any length and interval (provided they are multiples of the model's sampling period; see B for details).

The heat content of the inter-annually forced ACCESS-OM2 model 1° ocean model provided an illustrative example of the benefit of hat-averaging model budgets. In this model we expect a long-term build up of heat in the interior ocean due to increased thermal forcing from anthropogenic climate change. The heat content change computed using the snapshot difference between January 1st 1990 to January 1st 2010 was contrasted with an equivalent epoch difference which was computed using a 10 year epoch with the final epoch between 2005 to 2015 and the initial epoch between 1985 and 1995. The impact of variability on the boxcar-averaged tendency was highlighted by the presence of a moderate El Niño event at the end of the period of analysis. The snapshot difference over this period was strongly influenced by the El Niño event and a noisier spatial pattern of heat content change than that of the epoch difference, with substantial warming in the eastern Pacific. The vertical profile of the snapshot difference also showed a considerable warming anomaly in the upper 100 m of the ocean.

The benefit of hat-averaging is clear when we horizontally integrate the heat budget and remove a long-term control balance. Using a standard boxcar time-average, the change in heat content is strongly influenced by anomalous advection associated with vertical heaving of the equatorial Pacific during El Niño events, as advection varies strongly on short time-scales. In contrast, the impacts of this anomalous advection are reduced when considering the hat-averaged heat budget relating epoch differences that average over the ENSO cycle.

The application to the heat budget of an ocean model has shown hat-averaging to be appropriate for integrated quantities, particularly where we are interested in the contribution of various terms to a budget in the presence of a long-term trend. However, our results have also highlighted the difficulties and potential ambiguities involved in attributing changes in a property to changes in individual processes in the presence of large balances between processes. This constitutes a key area for future research.

*Code and data availability.*

Model code, configuration files, data processing scripts and processed data used in this study is available at https://doi.org/10.5281/zenodo.20798892 (Bladwell et al., 2026). Code for the hat averaging diagnostics implemented in MOM5 is available at
https://github.com/cbladwell/MOM5/commit/d25e3fbb553a4f4cc985f7f58d44ca8cf213721. Implementation of the hat average algorithm in MOM5 is contained in https://github.com/cbladwell/MOM5/blob/7e3b647/src/shared/diag_manager/diag_manager.F90.

https://doi.org/10.5194/egusphere-2026-3672
Preprint. Discussion started: 22 July 2026


## Appendix A: Proof of double integral formula

In this appendix we show equality between the double integral and the weighted integral used to define the hat average. This formula originates from Cauchy (1823). For a function $g$, the double integral formula is given by

$$\int_a^x \int_a^t g(s)\,\mathrm{d}s\,\mathrm{d}t = \int_a^x (x-t)\,g(t)\,\mathrm{d}t. \tag{A1}$$

where $t$ is within the interval $(a,x)$. To show equality, we begin with the left hand side of equation (A1). The Fundamental Theorem of Calculus (FTC) tells us for all $y$ in an interval $(a,b)$, if

$$G(y) = \int_a^y g(t)\mathrm{d}t,$$

then

$$G'(y) = g(y), \tag{A2}$$

and

$$\int_a^b g(t)\mathrm{d}t = G(b) - G(a). \tag{A3}$$

Applying the FTC to the left hand side of Eq. (A1), we obtain

$$\int_a^x \left[\int_a^t g(s)\,\mathrm{d}s\right]\,\mathrm{d}t = \int_a^x \left[G(t) - G(a)\right]\,\mathrm{d}t \tag{A4}$$

$$= \int_a^x G(t)\,\mathrm{d}t - xG(a) + aG(a), \tag{A5}$$

where we note that the integrand $G(a)$ is constant in $t$. We now apply integration by parts to the right hand side of Eq. (A1), which gives

$$\int_a^x (x-t)\,g(t)\,\mathrm{d}t = \int_a^x G'(t)\,(x-t)\,\mathrm{d}t \tag{A6}$$

$$= \int_a^x G(t)\,\mathrm{d}t + \Big[(x-t)\,G(t)\Big]_a^x \tag{A7}$$

$$= \int_a^x G(t)\,\mathrm{d}t - xG(a) + aG(a), \tag{A8}$$

which shows equality with the left hand side of equation (A1).

https://doi.org/10.5194/egusphere-2026-3672
Preprint. Discussion started: 22 July 2026


## Appendix B: Combining multiple hat averages

In this appendix we discuss the implementation of the hat average for a typical numerical model. To compute the hat-average either a rising or falling weighted average must be computed 'online' during the simulation at the model timestep, in addition to the standard unweighted average. Changes to the model's code are required to realize this functionality. As we show in this appendix, once both rising averages and conventional box-car averages of budget diagnostics are saved over the model diagnostic period (e.g. typically days or months), appropriate hat averages for longer periods (e.g. months or years, as long as those periods are simple combinations of the model diagnostic period) can be computed as a post processing step. In this section we describe how to combine multiple weighted integrals over the shorter model diagnostic period into a weighted integral over a longer period.

An example of this computation is illustrated in Figure B1. We consider a long epoch of interest $t \in (t_0, t_0 + \Delta T)$ split into $N$ shorter diagnostic periods of length $\Delta t$ (e.g. the month of January consists of $N = 31$ sections of length $\Delta t = 1$ day, with $\Delta T = N\Delta t$). For simplicity we consider these shorter diagnostic periods of equal length, however, the method can be applied even when the diagnostic periods have different length. The rising linearly weighted integral over the epoch $t \in (t_0, t_0 + \Delta T)$ (i.e. the first term in Eq. (9), blue in Fig. B1a) is given by,

$$\int_{t_0}^{t_0+N\Delta t} \frac{t-t_0}{N\Delta t}\frac{\partial \xi}{\partial t}dt = \int_{t_0}^{t_0+N\Delta t}\left[\frac{t-(t_0+(n-1)\Delta t)}{N\Delta t} + \frac{n-1}{N}\right]\frac{\partial \xi}{\partial t}dt \tag{B1}$$

$$= \sum_{n=1}^{N}\frac{1}{N}\int_{t_0+(n-1)\Delta t}^{t_0+n\Delta t}\frac{t-(t_0+(n-1)\Delta t)}{\Delta t}\frac{\partial \xi}{\partial t}dt$$

$$+\sum_{n=1}^{N}\frac{(n-1)}{N}\int_{t_0+(n-1)\Delta t}^{t_0+n\Delta t}\frac{\partial \xi}{\partial t}dt. \tag{B2}$$

The first term on the right hand side of Eq. (B2) is the sum of $1/N$ times the short rising difference over the short period (e.g. grey in Fig. B1a), and the second term is $(n-1)/N$ times the short standard difference over the short period (e.g. the red boxes in Fig. B1a).

The boxcar and falling integrals over the long epoch can be constructed similarly. The boxcar integral over the long epoch is trivially,

$$\int_{t_0}^{t_0+N\Delta t}\frac{\partial \xi}{\partial t}dt = \sum_{n=1}^{N}\int_{t_0+(n-1)\Delta t}^{t_0+n\Delta t}\frac{\partial \xi}{\partial t}dt, \tag{B3}$$

while the falling linearly weighted integral over the long epoch is equal to the difference between Eqs. (B3) and (B2).

$$\int_{t_0}^{t_0+N\Delta t}\frac{t_0+N\Delta t-t}{N\Delta t}\frac{\partial \xi}{\partial t}dt = \int_{t_0}^{t_0+N\Delta t}\frac{\partial \xi}{\partial t}dt - \int_{t_0}^{t_0+N\Delta t}\frac{t-t_0}{N\Delta t}\frac{\partial \xi}{\partial t}dt. \tag{B4}$$

https://doi.org/10.5194/egusphere-2026-3672
Preprint. Discussion started: 22 July 2026


Equation (B4) shows that the falling average can be computed by subtracting the rising average from the boxcar average multiplied by the elapsed time of the averaging period, as shown by the red and blue triangles between $(t_0, t_N + \Delta t)$ in Fig. B1b. This means that only the rising average and the standard average over the short diagnostic period ($\Delta t$) are required to construct hat averages (e.g. Eq. (9)) for any epoch length which is an integer multiple of the model output period (as shown by the blue region in Fig. B1b). We therefore recommend developers of climate models include the rising average as an option in addition to the boxcar average. This would also permit low-pass filtering with any form of truncated triangle convolution kernel.

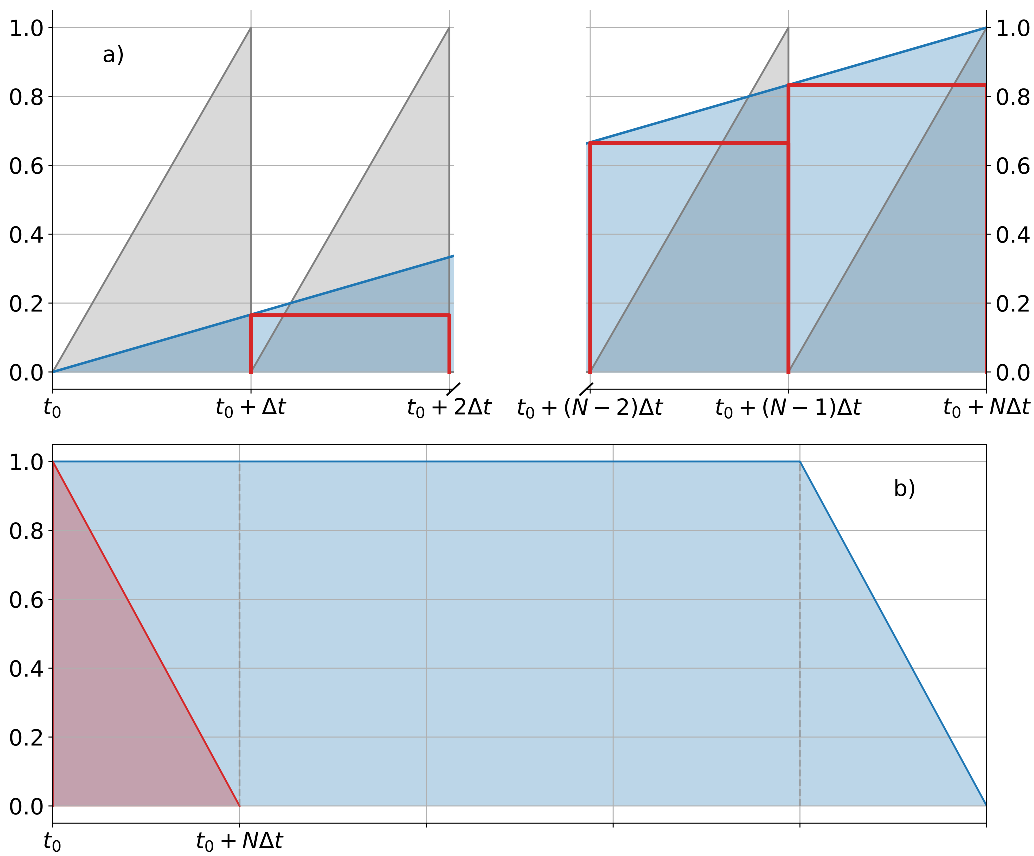


**Figure B1.** Schematic showing a) the weighting of multiple rising weighted averages over short periods (shown in grey), which can be combined into a single weighted average over a long period (shown in blue, where the diagonal lines indicate a break in the axis). b) Shows how an equivalent weighting to the hat-average can be constructed from two falling averages, which is given by Eq. (8) (the red shaded region is subtracted from the blue region).

https://doi.org/10.5194/egusphere-2026-3672
Preprint. Discussion started: 22 July 2026


*Author contributions.* All authors (CB,RH,JZ,SG,AK) contributed to the article content and text. CB developed code for the hat-averaging algorithm, ran the simulation and analysed the data. JZ and RH conceived the mathematical approach to the hat-average and application to ENSO. SG provided substantial insight into the model and many constructive discussions about the method. AK identified the frequency domain interpretation.

*Competing interests.* No authors have competing interests.

*Acknowledgements.* We thank the COSIMA community for their support of this work, and John Krasting at NOAA/GFDL for comments on an early draft. We also thank Sebastién Masson and Gurvan Madec for discussions. Modeling and analysis were undertaken using facilities at the National Computational Infrastructure (NCI) under the National Computational Merit Allocation Scheme, which is supported by the Australian Government. The authors are supported by the Australian Research Council (ARC)'s Centre of Excellence for Climate Extremes. The authors acknowledge support from the ARC through awards DP190101173 (J. Zika), DE21010004 (R. Holmes) and LP200100406 (A. Kiss). S. M. Griffies is funded through the France 2030 *Choose France for Science* program implemented by ANR (Agence Nationale de la Recherche) through CNRS at IPSL/LOCEAN (UMR7159, CNRS-IRD- MNHN-Sorbonne Université) in Paris.

https://doi.org/10.5194/egusphere-2026-3672
Preprint. Discussion started: 22 July 2026


## References

Barnes, E. A. and Barnes, R. J.: Estimating linear trends: simple linear regression versus epoch differences, Journal of Climate, 28, 9969–9976, 2015.

Bladwell, C., Holmes, R. M., Zika, J. D., Griffies, S. M., and Kiss, A. E.: Data, code and model configuration for a time-averaging algorithm applied to interannually-forced ACCESS-OM2 1° resolution model, https://doi.org/10.5281/zenodo.20798892, 2026.

Cauchy, A.-L.: Résumé des leçons données à l'école royale polytechnique sur le calcul infinitésimal, Imprimerie royale, 1823.

Deser, C., Phillips, A., Bourdette, V., and Teng, H.: Uncertainty in climate change projections: the role of internal variability, Climate dynamics, 38, 527–546, 2012.

Dias, F. B., Fiedler, R., Marsland, S., Domingues, C., Clément, L., Rintoul, S., Mcdonagh, E., Mata, M., and Savita, A.: Ocean heat storage in response to changing ocean circulation processes, Journal of Climate, 33, 9065–9082, 2020.

Ding, Q. and Steig, E. J.: Temperature change on the Antarctic Peninsula linked to the tropical Pacific, Journal of Climate, 26, 7570–7585, 2013.

Dong, B. and Dai, A.: The influence of the interdecadal Pacific oscillation on temperature and precipitation over the globe, Climate dynamics, 45, 2667–2681, 2015.

Fox-Kemper, B., Ferrari, R., and Hallberg, R.: Parameterization of mixed layer eddies. Part I: Theory and diagnosis, Journal of Physical Oceanography, 38, 1145–1165, 2008.

Gent, P. R. and McWilliams, J. C.: Isopycnal mixing in ocean circulation models, Journal of Physical Oceanography, 20, 150–155, 1990.

Gent, P. R., Willebrand, J., McDougall, T. J., and McWilliams, J. C.: Parameterizing eddy-induced tracer transports in ocean circulation models, Journal of Physical Oceanography, 25, 463–474, https://doi.org/10.1175/1520-0485(1995)025<0463:PEITTI>2.0.CO;2, 1995.

Gregory, J. M.: Vertical heat transports in the ocean and their effect on time-dependent climate change, Climate Dynamics, 16, 501–515, 2000.

Griffies, S. M.: The Gent-McWilliams Skew Flux, J. Phys. Oceanogr., 28, 831–841, https://doi.org/10.1175/1520-0485(1998)028<0831:TGMSF>2.0.CO;2, 1998.

Griffies, S. M.: Elements of the modular ocean model (MOM), GFDL Ocean Group Tech. Rep, 7, 620, 2012.

Griffies, S. M. and Greatbatch, R. J.: Physical processes that impact the evolution of global mean sea level in ocean climate models, Ocean Modelling, 51, 37–72, https://doi.org/10.1016/j.ocemod.2012.04.003, 2012.

Griffies, S. M., Gnanadesikan, A., Pacanowski, R. C., Larichev, V. D., Dukowicz, J. K., and Smith, R. D.: Isoneutral diffusion in a z-coordinate ocean model, Journal of Physical Oceanography, 28, 805–830, 1998.

Griffies, S. M., Winton, M., Anderson, W. G., Benson, R., Delworth, T. L., Dufour, C. O., Dunne, J. P., Goddard, P., Morrison, A. K., Rosati, A., et al.: Impacts on ocean heat from transient mesoscale eddies in a hierarchy of climate models, Journal of Climate, 28, 952–977, 2015.

Griffies, S. M., Danabasoglu, G., Durack, P. J., Adcroft, A. J., Balaji, V., Böning, C. W., Chassignet, E. P., Curchitser, E., Deshayes, J., Drange, H., Fox-Kemper, B., Gleckler, P., Gregory, J., Haak, H., Hallberg, R., Heimbach, P., Hewitt, H., Holland, D., Ilyina, T., Jungclaus, J., Komuro, Y., Krasting, J., Large, W., Marsland, S., Masina, S., McDougall, T., Nurser, A. G., Orr, J., Pirani, A., Qiao, F., Stouffer, R., Taylor, K., Treguier, A. M., Tsujino, H., Uotila, P., Valdivieso, M., Wang, Q., Winton, M., and Yeager, S.: OMIP contribution to CMIP6: experimental and diagnostic protocol for the physical component of the Ocean Model Intercomparison Project, Geoscientific Model Development, 9, 3231–3296, https://doi.org/10.5194/gmd-9-3231-2016, 2016.

https://doi.org/10.5194/egusphere-2026-3672
Preprint. Discussion started: 22 July 2026


Held, I. M., Winton, M., Takahashi, K., Delworth, T., Zeng, F., and Vallis, G. K.: Probing the fast and slow components of global warming by returning abruptly to preindustrial forcing, Journal of Climate, 23, 2418–2427, 2010.

Holmes, R. M., Sohail, T., and Zika, J. D.: Adiabatic and Diabatic Signatures of Ocean Temperature Variability, Journal of Climate, 35, 1459 – 1477, https://doi.org/10.1175/JCLI-D-21-0695.1, 2022.

Hunke, E. C., Lipscomb, W. H., Turner, A. K., Jeffery, N., and Elliott, S.: CICE: The Los Alamos Sea Ice Model Documentation and Software User's Manual Version 5.1, Tech. Rep. LA-CC-06-012, Los Alamos National Laboratory, 2015.

Jochum, M.: Impact of latitudinal variations in vertical diffusivity on climate simulations, Journal of Geophysical Research, 114 C01010, https://doi.org/10.1029/2008JC005030, 2009.

Kennedy, J. J., Rayner, N. A., Smith, R. O., Parker, D. E., and Saunby, M.: Reassessing biases and other uncertainties in sea surface temperature observations measured in situ since 1850: 2. Biases and homogenization, Journal of Geophysical Research: Atmospheres, 116, 2011.

Kiss, A. E., Hogg, A. M., Hannah, N., Boeira Dias, F., Brassington, G. B., Chamberlain, M. A., Chapman, C., Dobrohotoff, P., Domingues, C. M., Duran, E. R., et al.: ACCESS-OM2 v1.0: A global ocean–sea ice model at three resolutions, Geoscientific Model Development, 13, 401–442, 2020.

Klinger, B. A., Marshall, J., and Send, U.: Representation of convective plumes by vertical adjustment, Journal of Geophysical Research, 101, 18 175–18 182, https://doi.org/10.1029/96JC00861, 1996.

Kravitz, B., Lynch, C., Hartin, C., and Bond-Lamberty, B.: Exploring precipitation pattern scaling methodologies and robustness among CMIP5 models, Geoscientific Model Development, 10, 1889–1902, 2017.

Laliberté, F., Zika, J., Mudryk, L., Kushner, P., Kjellsson, J., and Döös, K.: Constrained work output of the moist atmospheric heat engine in a warming climate, Science, 347, 540–543, 2015.

Large, W. G., McWilliams, J. C., and Doney, S. C.: Oceanic vertical mixing: A review and a model with a nonlocal boundary layer parameterization, Reviews of geophysics, 32, 363–403, 1994.

Locarnini, R. A., Mishonov, A. V., Antonov, J. I., Boyer, T. P., Garcia, H. E., Baranova, O. K., Zweng, M. M., Paver, C. R., Reagan, J. R., Johnson, D. R., et al.: World ocean atlas 2013. Volume 1, Temperature, 2013.

McDougall, T. J.: Potential Enthalpy: A Conservative Oceanic Variable for Evaluating Heat Content and Heat Fluxes, J. Phys. Oceanogr., 33, 945–963, https://doi.org/10.1175/1520-0485(2003)033<0945:PEACOV>2.0.CO;2, 2003.

McDougall, T. J. and Barker, P. M.: Getting started TEOS-10 and the Gibbs Seawater (GSW) oceanographic toolbox, SCOR/IAPSO WG, 127, 1–28, 2011.

Morrison, A., Saenko, O., Hogg, A. M., and Spence, P.: The role of vertical eddy flux in Southern Ocean heat uptake, Geophysical Research Letters, 40, 5445–5450, 2013.

Oerder, V., Colas, F., Echevin, V., Masson, S., Hourdin, C., Jullien, S., Madec, G., and Lemarié, F.: Mesoscale SST–wind stress coupling in the Peru–Chile current system: Which mechanisms drive its seasonal variability?, Climate Dynamics, 47, 2309–2330, 2016.

Palter, J. B., Griffies, S. M., Galbraith, E. D., Gnanadesikan, A., Samuels, B. L., and Klocker, A.: The deep ocean buoyancy budget and its temporal variability, Journal of Climate, 27, 551–573, https://doi.org/10.1175/JCLI-D-13-00016.1, 2014.

Piecuch, C. G. and Ponte, R. M.: Mechanisms of global-mean steric sea level change, Journal of climate, 27, 824–834, 2014.

Redi, M. H.: Oceanic Isopycnal Mixing by Coordinate Rotation, J. Phys. Oceanogr., 12, 1154–1158, https://doi.org/10.1175/1520-0485(1982)012<1154:OIMBCR>2.0.CO;2, 1982.

Roemmich, D. and Gilson, J.: The global ocean imprint of ENSO, Geophys. Res. Lett., 38, https://doi.org/10.1029/2011GL047992, 2011.

https://doi.org/10.5194/egusphere-2026-3672
Preprint. Discussion started: 22 July 2026


Simmons, H. L., Jayne, S. R., Laurent, L. C. S., and Weaver, A. J.: Tidally driven mixing in a numerical model of the ocean general circulation, Ocean Model., 6, 245–263, https://doi.org/10.1016/S1463-5003(03)00011-8, 2004.

Tsujino, H., Urakawa, S., Nakano, H., Small, R. J., Kim, W. M., Yeager, S. G., Danabasoglu, G., Suzuki, T., Bamber, J. L., Bentsen, M., et al.: JRA-55 based surface dataset for driving ocean–sea-ice models (JRA55-do), Ocean Modelling, 130, 79–139, 2018.

Tsujino, H., Urakawa, L. S., Griffies, S. M., Danabasoglu, G., Adcroft, A. J., Amaral, A. E., Arsouze, T., Bentsen, M., Bernardello, R., Böning, C. W., et al.: Evaluation of global ocean–sea-ice model simulations based on the experimental protocols of the Ocean Model Intercomparison Project phase 2 (OMIP-2), Geoscientific Model Development, 13, 3643–3708, 2020.

Wolfe, C. L., Cessi, P., McClean, J. L., and Maltrud, M. E.: Vertical heat transport in eddying ocean models, Geophysical Research Letters, 35, 2008.

Zweng, M. M., Reagan, J. R., Antonov, J. I., Locarnini, R. A., Mishonov, A. V., Boyer, T. P., Garcia, H. E., Baranova, O. K., Johnson, D. R., Seidov, D., et al.: World ocean atlas 2013. Volume 2, Salinity, 2013.